2024 European Control Conference (ECC)
June 25-28, 2024. Stockholm, Sweden

Stability and Performance Assessment of a MIMO HIGS-based Controller Design

Ruud Beerens[1], Pieter Konings[2], Marcel Heertjes[1,2], Sebastiaan van den Eijnden[2]

***Abstract*— We present a frequency-domain stability analysis tool for the feedback interconnection of a linear time-invariant multi-input-multi-output plant and a nonlinear multi-input multi-output controller. The controller consists of several hybrid elements interconnected with well-crafted linear filters that together enable favourable phase properties and allow for improved controller performance. Stability and performance of the proposed controller design is evaluated on a wafer stage of an industrial metrology inspection machine.**

I. Introduction

Traditionally, motion systems in, e.g., wafer scanners and metrology inspection tools are controlled by proportional-integral-derivative (PID) control, despite the fact that these PID designs, or more generally speaking any linear time-invariant (LTI) control design, is subject to fundamental design limitations, see, e.g., [5]. Nowadays, these fundamental limitations pose a serious challenge as the growing demands on operational speed, accuracy, and robustness of industrial motion systems are becoming increasingly difficult to meet.

To potentially relax these obstructions and push the performance of high-tech motion systems beyond what is possible with LTI control, the field has witnessed a paradigm shift towards the use of nonlinear or hybrid controllers. A well-known early example is the Clegg integrator [3], which has spurred further developments into generalized reset elements and applications [1], [2], [9], [12], [17], nonlinear phase lead compensators [10] and hybrid integrator-gain systems (HIGS) [4], [7], [13]. Within the context of high-precision motion control, HIGS is of particular interest as, opposed to *discontinuous* control with traditional reset elements, it utilizes *continuous* control signals for enhancing, e.g, disturbance rejection properties and transient closed-loop response. Successful application of HIGS-based control for performance improvements in wafer scanners can be found in, e.g., [7], [15] and the references therein.

In all the aforementioned works, HIGS-based controller design has only been considered within a multi-loop single-input single-output (SISO) context. However, many practical motion control applications consist of multiple controlled directions, where mutivariable aspects such as cross-coupling between the controlled directions of the system plays a significant role. In this paper, we consider the HIGS-based controller design problem within a multi-input multi-output (MIMO) context. Specifically, we consider both stability and performance aspects during the design process, which in a nonlinear MIMO setting is not trivial.

At its basis, the HIGS-based controller design procedure that we propose in this paper relies on the SISO approach outlined in [7, Sec. IV], where the describing function approximation of HIGS is embedded within a classical loop-shaping framework. Although such a describing function method is useful for frequency-domain design of nonlinear controllers, only stability *indications* can be provided by such an approximation in the frequency domain by, e.g., evaluating the quasi-linear Nyquist criterion. A rigorous stability analysis of HIGS-based controllers can instead be provided through numerically tractable linear matrix inequalities (LMIs), see, e.g., [15]. Such an analysis, however, requires a sufficiently accurate parametric model of complex systems which may not be easy to obtain. In order to favor industrialization of HIGS-based controllers, we present frequency-domain conditions for a stability analysis of MIMO control systems with a HIGS-based integrator [15, Sec. 3.2] for each controlled direction. These frequency domain conditions are based on a nontrivial description of the closed-loop system, eventually exploiting the multivariable circle criterion, and can hence be verified graphically using *measured* frequency response data of the considered system. The developments in this paper build upon the analysis presented in [16], where only SISO systems and a specific HIGS-based configuration is addressed, that fundamentally differs from the HIGS-based integrator configuration considered in this paper.

The main contributions of this paper are 1) a frequency-domain tool for stability analysis of MIMO HIGS-based control systems, and 2) an experimental performance assessment of a HIGS-based control design on a MIMO wafer stage of an industrial metrology inspection machine.

The remainder of this paper is organized as follows. We present our MIMO HIGS-based controller design in Section II and discuss the closed-loop setting in Section III. Our main results are presented in Section IV and Section V in the form of, respectively, a frequency-domain stability condition, and an experimental performance assessment. Conclusions are provided in Section VI

II. HIGS-based control

We consider a nonlinear controller design where we employ a HIGS-based integrator instead of a linear integrator in a PID-type filter. Before introducing the nonlinear controller structure, we present the HIGS element $\mathcal{H}$ as the following

Part of the research leading to these results has received funding from the European Research Council under the Advanced ERC Grant Agreement PROACTHIS, no. 101055384.

[1] ASML, De Run 6501, 5505DR Veldhoven, The Netherlands.
[2] Eindhoven University of Technology, Department of Mechanical Engineering, P.O. Box 513, 5600MB Eindhoven, The Netherlands.
ruud.beerens-rbkg@asml.com, m.f.heertjes@tue.nl
s.j.a.m.v.d.eijnden@tue.nl.

piecewise linear system:

$$\mathcal{H}:\begin{cases}\dot{x}_h = \omega_h z, & \text{if } (z,u_h,\dot{z})\in\mathcal{F}_1, \quad (1a)\\ x_h = k_h z, & \text{if } (z,u_h,\dot{z})\in\mathcal{F}_2, \quad (1b)\\ u_h = x_h, & \quad (1c)\end{cases}$$

with state $x_h \in \mathbb{R}$, $z \in \mathbb{R}$ the input (with $\dot{z}$ its time derivative), and $u_h \in \mathbb{R}$ the generated output. The integrator frequency $\omega_h \in (0,\infty)$ and gain $k_h \in (0,\infty)$ are tuning parameters.

The main philosophy of HIGS is to keep the sign of the integrator output u_h equal to the sign of the input z at all times by switching between two modes of operation, i.e., *integrator mode* according to (1a), and *gain mode* according to (1b). Integrator mode (the primary mode of operation) is allowed as long as the input-output pair (z,u_h) resides inside the sector $[0,k_h]$ in the (z,u_h)-plane defined as

$$\mathcal{F} := \left\{(z,u_h,\dot{z})\in\mathbb{R}^3 \mid zu_h \geq \frac{1}{k_h}u_h^2\right\}. \quad (2)$$

Note that the definition of $\mathcal{F}$ in (2) requires a suitable initialization of $z(0)\in\mathcal{F}$. A switch from integrator mode to gain mode occurs as soon as the trajectory tends to escape the sector $[0,k_h]$, whereby the trajectory slides over the boundary according to (1b). Conversely, a transition from gain mode back to integrator mode occurs whenever the vector field points towards the interior of $\mathcal{F}$. Switching is governed by the sets $\mathcal{F}_1$ and $\mathcal{F}_2$, i.e.,

$$\mathcal{F}_1 := \{(z,u_h,\dot{z})\in\mathbb{R}^3 \mid k_h z u_h \geq u_h^2 \wedge z\notin\mathcal{F}_2\}, \quad (3a)$$
$$\mathcal{F}_2 := \{(z,u_h,\dot{z})\in\mathbb{R}^3 \mid u_h = k_h z \wedge \omega_h z^2 > k_h \dot{z} z\}. \quad (3b)$$

A quasi-linear approximation of the HIGS element $\mathcal{H}$ in the frequency domain can be obtained by its first-order describing function, given by

$$\mathcal{D}(j\omega) = \frac{\omega_h}{j\omega}\left(\frac{\gamma}{\pi} + j\frac{e^{-2j\gamma}-1}{2\pi} - 4j\frac{e^{-j\gamma}-1}{2\pi}\right) + k_h\left(\frac{\pi-\gamma}{\pi} + j\frac{e^{-2j\gamma}-1}{2\pi}\right), \quad (4)$$

with $\gamma = 2\operatorname{atan}\left(\frac{k_h\omega}{\omega_h}\right) \in [0,\pi]$ the periodic switching instance between integrator mode and gain mode. The describing function (4) reveals that the HIGS element experiences first-order low-pass filter magnitude characteristics in the frequency domain, where the induced phase lag is only 38.15 degrees (in contrast to a classical, linear low-pass filter, inducing 90 degrees phase lag), see Fig. 1.

With the definition of the HIGS element $\mathcal{H}$ and its describing function $\mathcal{D}$ in place, we construct a HIGS-based integrator $\mathcal{C}_i\{\mathcal{H}\}$, following the rationale as in [15, Sec. 3.2]. Take $k_h = 1$, and perform a pre- and post-multiplication of $\mathcal{H}$ with a lead filter $\mathcal{T}_1 := (s+\omega_N)/\omega_N$, with $\omega_N := \omega_h\,|1+4j/\pi|$, and simple integrator $\mathcal{T}_2 := \omega_i/s$, respectively, i.e.,

$$\mathcal{C}_i\{\mathcal{H}\} := \mathcal{T}_1(s)\mathcal{L}\{\mathcal{H}(z,\dot{z},u_h)\}\mathcal{T}_2(s), \quad (5)$$

with $s\in\mathbb{C}$, and $\mathcal{L}$ denotes the Laplace transform of $\mathcal{H}$ on the input signals z, $\dot{z}$, and u_h. The design philosophy for the HIGS-based integrator (5), illustrated in Fig. 2, stems from

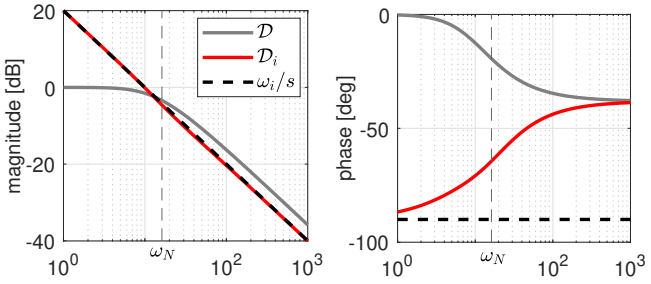

Fig. 1. Bode diagrams of the describing functions $\mathcal{D}(j\omega)$ of the HIGS element $\mathcal{H}$ (with corner frequency $\omega_N := k_h^{-1}\omega_h\,|1+4j/\pi|$), $\mathcal{D}_i(j\omega)$ of the HIGS-based integrator $\mathcal{C}_i\{H\}$, and a linear integrator.

describing function analysis. Indeed, a describing function for the HIGS-based integrator $\mathcal{C}_i$ is given by $\mathcal{D}_i(j\omega) := \mathcal{T}_1(j\omega)\mathcal{D}(j\omega)\mathcal{T}_2(j\omega)$, which yields precisely the magnitude characteristic of a classical integrator, but with (locally) reduced phase lag, see Fig. 1. This phase benefit is the key mechanism to (transient) performance improvements for high-tech systems, as we illustrate in Section V below. Moreover, the state of the simple integrator in $\mathcal{C}_i$ ensures that the HIGS-based integrator is capable of sustaining a DC output, which is not possible for the HIGS element $\mathcal{H}$ in (1).

Consider Fig. 2, where we introduce the HIGS-based controller structure, and a representation of the controller in feedback with an LTI plant $\mathcal{P}$. For the sake of brevity, the representation is given for a single DOF, but naturally extends to a MIMO context by considering each filter as a diagonal matrix, and each signal as a time-varying vector of suitable dimensions (as we formalize in the next section). Next to the HIGS-based integrator $\mathcal{C}_i$, the controller consists of a second order low-pass filter $\mathcal{C}_{lp}$, and a parallel PD branch (with differentiator frequency ω_d). Note that this controller structure mimics a classial PID-type controller design, where we have replaced a classical integrator by the HIGS-based one.

Remark 1. *The considered PID-type controller structure as depicted in Fig. 2 can be trivially extended with a series of Notch filters, commonly used in high-tech motion systems.*

Remark 2. *In order to avoid known problems in a HIGS-based controller design such as* gain loss *associated with too frequent switching of HIGS, a pre-and post filtering strategy is applied in the design, see [8].*

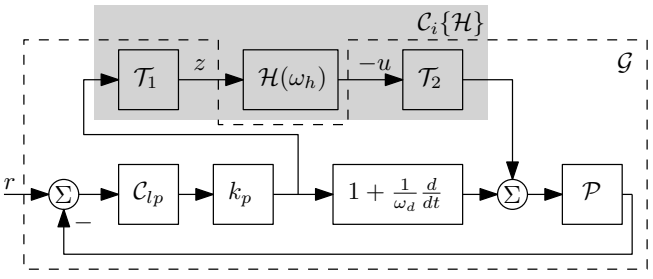

Fig. 2. Closed-loop HIGS-based control structure consisting of a second-order low-pass filter $\mathcal{C}_{lp}$, and a PD branch parallel to a HIGS-based integrator $\mathcal{C}_i\{\mathcal{H}\}$.

III. Closed-loop system description

The MIMO representation of the closed-loop HIGS-based control system depicted in Fig. 2, with m controlled directions, is rewritten as the feedback interconnection of a MIMO LTI system $\mathcal{G} \in \mathbb{R}^{m\times m}$ and a matrix $\bar{\mathcal{H}} \in \mathbb{R}^{m\times m}$, with the individual HIGS elements on the diagonal, see Fig. 3. The LTI system $\mathcal{G}$ is given by

$$\mathcal{G}: \begin{cases} \dot{x}_l = A_l x_l + B_l u + B_r r, & (6) \\ z = C_l x_l + D_l u, & (7) \end{cases}$$

with state vector $x_l \in \mathbb{R}^n$, output $z \in \mathbb{R}^m$, exogenous input $r \in \mathbb{R}^m$, and control input $u \in \mathbb{R}^m$. The corresponding transfer functions from u to z, and from r to z are given by

$$\mathcal{G}_{zu}(s) = C_l(sI - A_l)^{-1}B_l + D_l, \quad (8a)$$
$$\mathcal{G}_{zr}(s) = C_l(sI - A_l)^{-1}B_r, \quad (8b)$$

respectively, on which we pose the following assumption:

Assumption 1. *The transfer functions $\mathcal{G}_{zu}$ and $\mathcal{G}_{zr}$ have a relative degree of at least two, and $\mathcal{G}_{zu}$ is observable.*

Assumption 1 is considered mild, since mechanical motion systems are typically described by double integrators with additional dynamics, which naturally leads to a relative degree of at least two. A consequence of Assumption 1 is that $D_l = 0$ and $C_l B_l = C_l B_r = 0$.

Each HIGS element in the closed-loop system satisfies (1) with $k_h = 1$[†]. With multiple HIGS elements present in the considered system, we reformulate each individual HIGS element to have an appropriate definition in a MIMO motion control context, and we adopt a different definition for the gain mode. That is, the i-th HIGS element, for $i \in \{1, \dots, m\}$, satisfies

$$\mathcal{H}_i: \begin{cases} \dot{x}_{h,i} = \omega_{h,i} z_i, \quad \text{if } (z_i, \dot{z}_i, u_{h,i}) \in \mathcal{F}_{1,i}, & (9a) \\ \dot{x}_{h,i} = \dot{z}_i + \lambda_i (x_{h,i} - z_i), & (9b) \\ \qquad\qquad \text{if } (z_i, \dot{z}_i, u_{h,i}) \in \mathcal{F}_{2,i}, \end{cases}$$

with the set definitions for $\mathcal{F}_{1,i}$ and $\mathcal{F}_{2,i}$ equivalent to the definitions in (3), $x_h := [x_{h,1}, \dots, x_{h,m}]^\top$, $z := [z_1, \dots, z_m]^\top$, and $u := -x_h$. In addition, the HIGS frequencies $\omega_{h,i}$ are collected in a diagonal matrix Ω_h, denoted by $\Omega_h := \mathrm{diag}([\omega_{h,1}, \dots, \omega_{h,m}]^\top)$.

Observe the slightly different definition of gain mode in (9b), compared to (1b). In (9b), we differentiate (1b) with respect to time, and add an extra term $\lambda_i(x_{h,i} - z_i)$, with $\lambda_i \in \mathbb{R} \setminus \{0\}$. This term is zero for $(z_i, \dot{z}_i, u_{h,i}) \in \mathcal{F}_{2,i}$, and thus may be added to the gain-mode characteristics without changing the dynamics. In particular, the term $\lambda(x_{h,i} - z_i)$ achieves avoiding the open-loop having one or more poles on the imaginary axis when HIGS is in gain mode, which is instrumental for the stability analysis presented in the next section.

[†]Without loss of generality we set $k_h = 1$ in HIGS. Because of homogeneity of the dynamics, the gain is then incorporated into the gain of $\mathcal{T}_2$.

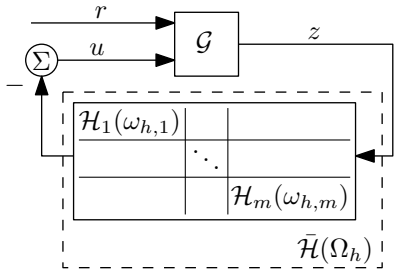

Fig. 3. Lur'e-type feedback interconnection of the MIMO HIGS-based control system, with LTI part $\mathcal{G}$ and HIGS elements $\bar{\mathcal{H}}$.

For the purpose of constructing the frequency-domain stability analysis tools, we include the linear integrator/gain mode dynamics of each HIGS element $\mathcal{H}_i$, according to (9), in the linear part of the closed-loop system, and describe the state-dependent switching between these gain and integrator modes of the subsequent HIGS elements by an "on/off" switch, as considered before in [16]. Specifically, we rewrite the closed-loop representation of Fig. 3 as follows:

$$\Sigma: \begin{cases} \dot{x} = Ax + Bw + B_r r, & (10a) \\ y = Cx, & (10b) \\ w = \Phi(x) y, & (10c) \end{cases}$$

with $x := [x_l^\top, x_h^\top]^\top$, and where the switching between integrator mode and gain mode for each HIGS element is governed by a state-dependent switching law Φ, on which we now elaborate further. With the definition $\Lambda := \mathrm{diag}([\lambda_1, \dots, \lambda_m]^\top)$, the system matrix A in (10) is given by

$$A := \begin{bmatrix} A_l & B_l \\ C_l A_l - \Lambda C_l & \Lambda \end{bmatrix}. \quad (11)$$

Moreover, the matrices B and C in (10) are given by

$$B := \begin{bmatrix} 0^{m\times n} & I^m \end{bmatrix}^\top. \quad (12a)$$
$$C := \begin{bmatrix} \Omega_h C_l - C_l A_l + \Lambda C_l & -\Lambda \end{bmatrix}, \quad (12b)$$

with I^m the $m \times m$ identity matrix. The matrix $\Phi := \mathrm{diag}([\phi_1, \dots, \phi_m]^\top)$ contains on its diagonal the "on/off"-type switches $\phi_i \in [0, 1]$ for each HIGS element $\mathcal{H}_i$. In particular, for $\phi_i = 0$ the considered element is in *gain mode*, and for $\phi_i = 1$ in *integrator mode*, i.e.,

$$\phi_i := \begin{cases} 1, & \text{if } (z_i, \dot{z}_i, u_{h,i}) \in \mathcal{F}_{1,i}, \quad (13a) \\ 0, & \text{if } (z_i, \dot{z}_i, u_{h,i}) \in \mathcal{F}_{2,i}. \quad (13b) \end{cases}$$

Using the definition of HIGS in (9) (instead of the one in (1)) leads to the matrix A in (11) having nonzero eigenvalues. This property is instrumental in the stability analysis of Section IV below.

IV. Frequency-domain stability analysis

In this section, we present sufficient frequency-domain conditions for input-to-state stability of closed-loop system (10)-(13) according to the next definition.

Definition 1. *The closed-loop system* (10)-(13) *is input-to-state stable (ISS) if there exist a $\mathcal{KL}$-function α and $\mathcal{K}$-function β such that, for any initial condition $x_l(0) \in \mathbb{R}^n$,*

and, for each $i \in \{1, \ldots, m\}$, $x_{h,i}(0) \in \mathcal{F}_{1,i} \cup \mathcal{F}_{2,i}$, *for any bounded input signal* r, *all solutions to* (10)-(13) *satisfy*

$$\|x(t)\| \leq \alpha(\|x(0)\|, t) + \beta\left(\sup_{0 \leq \tau \leq t} \|r(\tau)\|\right), \qquad (14)$$

for all $t \geq 0$.

Locally absolutely continuous solutions to (10)-(13) exist for all $t \geq 0$ by the developments in [6]. We are now ready to pose our main theorem:

Theorem 1. *Suppose that Assumption 1 and the following conditions hold:*

1) *The matrix* $Q(j\omega)+Q(j\omega)^*$ *with* $Q(j\omega) := I+W(j\omega)$, *and where*

$$W(j\omega) := ((\mathcal{V}_2(j\omega) - \Lambda)\mathcal{G}_{zu}(j\omega)(I+ \mathcal{G}_{zu}(j\omega))^{-1} + \Lambda)\,\mathcal{V}_1(j\omega), \qquad (15)$$

with $\mathcal{V}_1(j\omega) = (j\omega I - \Lambda)^{-1}$, *and* $\mathcal{V}_2(j\omega) = \Omega_h - j\omega I + \Lambda$, *is positive definite for all* $\omega \in \mathbb{R} \cup \{\infty\}$.

2) W *is Hurwitz.*

Then, the closed-loop system (10)-(13) *is ISS.*

Proof: see Appendix I.

The second condition in Theorem 1 amounts to a stable closed loop when all HIGS elements reside in *gain mode*, i.e., $\Phi = 0$, which can be satisfied by design. Specifically, the condition is satisfied as long as the system matrix A in (11) is Hurwitz, which, in turn requires the description for HIGS as in (9) with $\lambda_i < 0$. Indeed, it is easy to see that using the description for HIGS in (1) would result in the matrix A having at least one zero eigenvalue.

Both conditions in the theorem can be verified graphically based on known frequency response functions, and measured frequency response data of the plant $\mathcal{P}$. To elaborate on the origin of these conditions, let us consider the following rationale. The input to the nonlinear logic Φ is denoted by $y = Cx = \Omega_h z - \dot{z} + \Lambda(z - x_h)$, whereas its output is given by $w = \Phi(x)y = \Phi(x)Cx$. Furthermore, note that the dynamics of the HIGS elements x_h can be expressed as $\dot{x}_h = \Lambda x_h + \dot{z} - \Lambda z + w$, which, in terms of a transfer function representation can be written as

$$x_h = z + \mathcal{V}_1(s)w, \quad \text{with} \quad \mathcal{V}_1(s) = (sI - \Lambda)^{-1}. \qquad (16)$$

Recall that $w = \Phi(x)y$ and $y = \mathcal{V}_2(s)z - \Lambda x_h$ with $\mathcal{V}_2(s) = \Omega_h - sI + \Lambda$, and $u = -x_h$. With these ingredients in place, we see from Fig. 4 that the transfer function from w to y is given by

$$W(s) := ((\mathcal{V}_2(s) - \Lambda)\mathcal{G}_{zu}(s)(I+ \mathcal{G}_{zu}(s))^{-1} + \Lambda)\,\mathcal{V}_1(s). \qquad (17)$$

Since Φ is a diagonal matrix for which the elements are either zero or one, we can essentially apply the circle-criterion [11] to guarantee stability of the closed-loop system in Fig. 4. This amounts to verifying whether the transfer function matrix $W(s) + I$ is strictly positive real, which exactly corresponds to the conditions in Theorem 1.

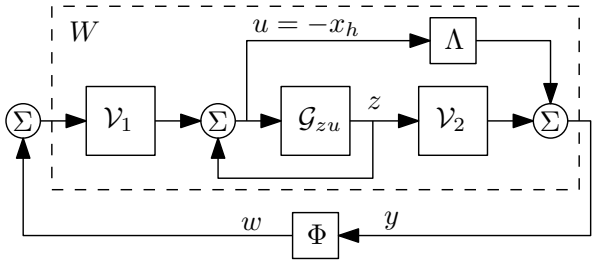

Fig. 4. Lur'e-type feedback interconnection of system (10)-(13), with LTI part W and switching logic Φ.

V. Performance Analysis

In this section, we experimentally illustrate the performance benefits of the HIGS-based controller compared to its linear counterpart, by applying it to a state-of-the-art metrology inspection tool.

A. Metrology Inspection Tool

Modern microchips, fabricated through a photolithographic process [7], can contain up to 100 layers, which all need to align on top of each other as accurately as possible. Such an overlay property is monitored by a metrology inspection machine, which contains a moving wafer stage (on which we focus in this paper) that positions the wafer under an optical sensor. The sensor measures overlay by emitting light onto specific markers at several locations on a wafer, and measures back the diffraction pattern. The intensity difference of the scattered light pattern results in a metric for overlay accuracy.

A large amount of markers, spread across the complete wafer surface, are positioned under the sensor through a sequence of point-to-point motion profiles of the wafer stage from one marker to the next, where stringent requirements on settling time are imposed to maximize machine throughput. Once the stage has settled within an allowable positioning error bound, the optical sensor can perform an overlay measurement (i.e., *acquirement*), after which the stage moves to the next marker. Control performance can, therefore, be expressed in terms of overshoot and settling time.

A schematic representation of the wafer stage of a modern metrology inspection machine is presented in Figure 5. The stage consists of two perpendicular beams to which a wafer carrier is attached. Actuators are located at either end of the beams, and a mapping from the point-of-interest (i.e., the point on the wafer that lies under the optical sensor) to actuator forces is employed, allowing us to control the logical x and y directions of the point-of-interest. Although the resulting MIMO plant is dominantly diagonal, cross-talk is still evidently present due to the presence of low-frequency stiffness effects and high-frequency dynamics, illustrated by the relative gain array (see [14, Sec. 3.6]) in Fig. 6. We take this multivariable aspect explicitly into account in the (nonlinear) feedback controller design. Furthermore, we emphasize that a suitable multi-loop SISO feedforward controller is taken into account, comprising of mass feedforward (including delay compensation), and compliance compensation.

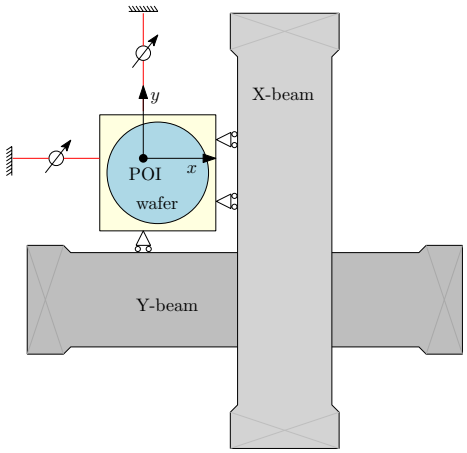

Fig. 5. Schematic representation of a wafer stage of a metrology inspection tool. The stage is driven by four actuators at either side of the X-beam and Y-beam. The point-of-interest (POI) position is measured by interferometers.

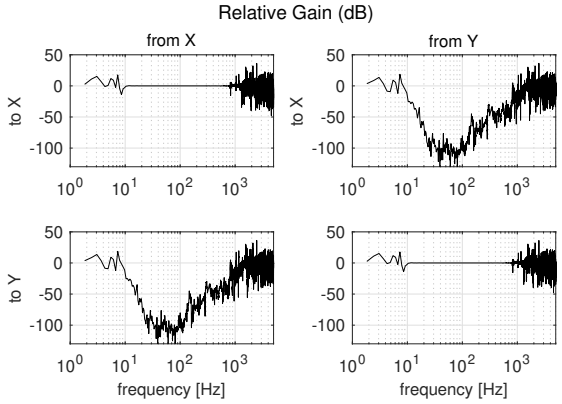

Fig. 6. Relative Gain Array of the MIMO wafer stage system, indicating low and high-frequency cross-talk between the controlled directions.

B. Nonlinear controller design and stability assessment

The purpose of the experimental case study is to demonstrate the (transient) performance improvements that can be obtained by the HIGS-based controller, compared to its linear counterpart. First, we design a diagonal *linear* PID-type controller consisting of a PID filter, a second-order low-pass filter, and a series of Notch filters, using an automated H_∞ loopshaping procedure, explicitly taking into account any cross-talk between the logical controlled directions x and y. Trivially, for such linear controller design, closed-loop system stability is achieved by evaluation of the generalized Nyquist criterion.

Next, we replace the linear integrator in the PID filter by the HIGS-based equivalent in (5), where we keep the same controller parameter values as for the linear case. In addition, we aim to tune the HIGS parameters in Ω_h in such a way that stability is guaranteed through satisfaction of the conditions in Theorem 1, and such that it achieves satisfactory time-domain performance. In particular, condition 1) of Theorem 1 is verified graphically by evaluating the eigenvalues of $Q(j\omega) + Q(j\omega)^*$ in Fig. 7(a), which reveals strictly positive eigenvalues for all ω, thereby satisfying the condition. Condition 2) can be verified by evaluating the characteristic loci of the open loop of W, given by

$$\mathcal{O}_W := (sI - \Lambda)\mathcal{G}_{zu}\frac{1}{s}I - \Lambda\frac{1}{s}I. \tag{18}$$

The characteristic loci of $\mathcal{O}_W$, where we select $\Lambda = -20I$, are presented in Fig. 7(b), from which we conclude that $W(j\omega)$ is Hurwitz since there are no encirclements of the point $(-1, 0)$.

Finally, in order to achieve a correct switching behavior of the HIGS element, we employ pre- and post filtering of the HIGS elements to avoid loop gain loss (cf. Remark 2), see [8].

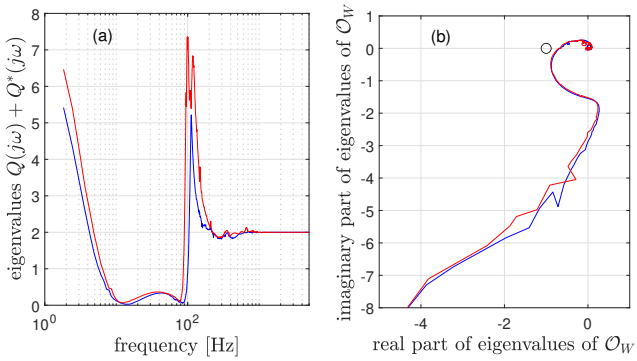

Fig. 7. Graphical verification of the stability conditions of Theorem 1.

C. Comparative performance analysis

Consider Fig. 8, which presents the positioning errors for a series of point-to-point wafer stage moves in combined x and y direction. A scaled acceleration reference is visualized, the end of which is indicated by "move end". When the setpoint has finished, the stage is allowed 5ms settling time before a measurement of a marker takes place (indicated by "settling end"). Such a measurement (or acquirement) may take up to 22.5ms (indicated by "acquirement end"), so that a high accuracy is required within the time interval $[0.005, 0.0275]$ s. The required accuracy is indicated by the horizontal black dashed lines.

Observe that, for the linear controller, the maximum allowable settling time is exceeded due to overshooting the setpoint. Instead, the HIGS-based controller significantly reduces overshoot in both logical directions due to the phase advantages of the HIGS integrator, thereby achieving a significant settling time reduction. Moreover, such overshoot reduction leads to a reduced peak-to-peak error after "settling end" by a factor 2, resulting in improved measurement quality.

For the considered use case, the HIGS parameters $\omega_{h,i}$ (for both the x and y controller) are tuned such that settling time is minimized and accuracy is achieved during acquirement. Although the HIGS controller clearly realizes this goal, a larger error during deceleration can be observed due to some remaining loop gain loss caused by the interplay of the pre- and post filters [8] and the relatively low value for $\omega_{h,i}$. A possible solution to reduce such gain loss, and improve performance even further, is to increase the HIGS parameters $\omega_{h,i}$.

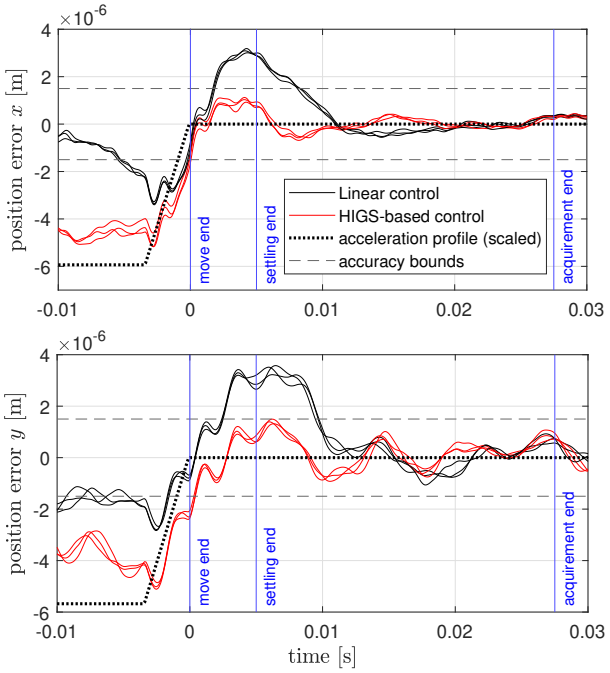

Fig. 8. Measured position errors after a typical combined x-y wafer stage move for the linear controller (black), and a HIGS-based controller (red).

VI. Conclusion

We have presented frequency-domain stability conditions for nonlinear multivariable control systems with HIGS-based integrators. The stability conditions can be checked graphically, which is illustrated by a HIGS-based controller design for an industrial metrology inspection machine. The performance benefits of the HIGS-based controller is experimentally validated. Future work encompasses reduction of conservatism and extension of the stability tools towards more generic HIGS-based controller designs.

Appendix I: Proof of Theorem 1

The conditions of the theorem amount to the transfer function $Q(s) := I + W(s)$ being strictly positive real. Under the hypothesis stated in the theorem, by virtue of the Kalman-Yakubovich-Popov Lemma [11, Lemma 6.3], there exists $P = P^\top > 0$, L, and $\varepsilon > 0$ such that

$$A^\top P + PA = -L^\top L - \varepsilon P, \tag{19a}$$

$$PB = -C^\top + \sqrt{2}L^\top. \tag{19b}$$

Consider the quadratic candiate ISS-Lyapunov function $V = x^\top Px$, for which $V(x) > 0$ for all $x \neq 0$. Its time derivative along solutions of (10)-(13) is given by

$$\begin{aligned}\dot{V} &= -x^\top L^\top Lx - \varepsilon V - 2x^\top \left(C^\top - \sqrt{2}L^\top\right) w \\ &\qquad + 2x^\top PB_r r \\ &= -x^\top L^\top Lx - \varepsilon V - 2\left(Cx - w\right)^\top w - 2w^\top w \\ &\qquad + 2\sqrt{2}x^\top L^\top w + 2x^\top PB_r r \\ &= -\left(Lx - \sqrt{2}w\right)^\top \left(Lx - \sqrt{2}w\right) - 2\left(Cx \right. \\ &\qquad \left. - w\right)^\top w - \varepsilon V + 2x^\top PB_r r \\ &\leq -\varepsilon V = -2\left(Cx - w\right)^\top w + 2x^\top PB_r r \\ &= -\varepsilon V - 2x^\top C^\top w + 2w^\top w + 2x^\top PB_r r.\end{aligned}$$

Using the equalities in (19), $w = \Phi(x)y$, and $y = Cx$, $\dot{V}$ yields

$$\begin{aligned}\dot{V} &= -\varepsilon V - 2x^\top C^\top \Phi(x) Cx \\ &\qquad + 2x^\top C^\top \Phi(x)\Phi(x) Cx + 2x^\top PB_r r \\ &= -\varepsilon V + 2x^\top PB_r r,\end{aligned}$$

where we have used the identity $\Phi(x)\Phi(x) = \Phi(x) \geq 0$. Let $\overline{\lambda}(P)$ and $\underline{\lambda}(P)$ denote the largest and smallest eigenvalue of P, respectively. Then, an upper bound for $\dot{V}$ is given by

$$\begin{aligned}\dot{V} &\leq -\varepsilon \underline{\lambda}(P)\|x\|^2 + 2\|PB_r\|\|x\|\|r\| \\ &\leq \mu\|x\|^2 + \gamma\|r\|^2,\end{aligned}$$

with $\mu := \varepsilon\underline{\lambda}(P) - \delta$, $\gamma := \sqrt{\frac{\overline{\lambda}(P)}{\underline{\lambda}(P)}}\frac{2\|PB_r\|}{\delta}$, and δ such that $0 < \delta < \varepsilon\underline{\lambda}(P)$.

References

[1] W. Aangenent, G. Witvoet, W.P.M.H. Heemels, M. van de Molengraft, and M. Steinbuch. Performance analysis of reset control systems. *Int. J. of Robust and Nonlinear Control*, 20:1213–1233, 2010.

[2] R. Beerens, A. Bisoff, L. Zaccarian, W.P.M.H. Heemels, H. Nijmeijer, and N. van de Wouw. Reset integral control for improved settling of pid-based motion systems with friction. *Automatica*, 107:483–492, 2019.

[3] J. Clegg. A nonlinear integrator for servomechanisms. *Transactions of the American Institute of Electrical Engineers Pt. II*, 77:41–42, 1958.

[4] D.A. Deenen, B. Sharif, S.J.A.M. van den Eijnden, H. Nijmeijer, W.P.M.H. Heemels, and M.F. Heertjes. Projection-based integrators for improved motion control: formalization, well-posedness and stability of hybrid integrator-gain systems. *Automatica*, 133, 2021.

[5] J. Freudenberg, R. Middleton, and A. Stefanpoulou. A survey of inherent design limitations. *Proc. 2000 American Control Conference (ACC)*, pages 2987–3001, 2000.

[6] W.P.M.H. Heemels and A. Tanwani. Existence and completeness of solutions to extended projected dynamical systems and sector-bounded projection-based controllers. *Control Syst. Lett.*, 7:1590–1595, 2023.

[7] M. Heertjes, S. van den Eijnden, and B. Sharif. An overview on hybrid integrator-gain systems with applications to wafer scanners. *Proc. 2023 International Conference on Mechatronics (ICM)*, 2023.

[8] M.F. Heertjes, S.J.A.M. van den Eijnden, W.P.M.H. Heemels, and H. Nijmeijer. A solution to gain loss in hybrid integrator-gain systems. *Proc. 2021 Conference on Control Technology and Applications (CCTA)*, pages 1179–1184, 2021.

[9] I. Horowitz and P. Rosenbaum. Non-linear design for cost of feedback reduction in systems with large parameter uncertainty. *Int. J. Control*, 21:977–1001, 1975.

[10] N. Karbasizadeh and S. Hassan HosseinNia. Continuous reset element: transient and steady-state analysis for precision motion systems. *Control Engineering Practice*, 126, 2022.

[11] K.H. Khalil. *Nonlinear systems*. Pearson, 2002.

[12] D. Nešić, A. Teel, and L. Zaccarian. Stability properties of reset systems. *Automatica*, 82:2019–2026, 2008.

[13] Kanghong Shi, Nastaran Nikooienejad, Ian R. Petersen, and S. O. Reza Moheimani. A negative imaginary approach to hybrid integrator-gain system control. *Proc. 2022 Conference on Decision and Control (CDC)*, pages 1968–1973, 2022.

[14] S. Skogestad and I. Postlethwaite. *Multivariable feedback control: analysis and design*. Wiley and sons, 2010.

[15] S. van den Eijnden, M. Francke, Nijmeijer H., and M. Heertjes. Improving wafer stage performance with multiple hybrid integrator-gain systems. *IFAC PapersOnline*, 32:8321–8326, 2020.

[16] S.J.A.M. van den Eijnden, M.F. Heertjes, W.P.M.H. Heemels, and H. Nijmeijer. Frequency-domain tools for stability analysis of hybrid integrator-gain systems.

[17] S. van Loon, K. Gruntjes, M. Heertjes, N. van de Wouw, and M. Heemels. Frequency-domain tools for stability analysis of reset control systems. *Automatica*, 82:101–108, 2017.